EUDET-Memo-2008-09

Redefinition of the Geometry of the Luminosity Calorimeter

H. Abramowicz, R. Ingbir, S. Kananov, A. Levy, I. Sadeh

School of Physics and Astronomy, The Raymond and Beverly Sackler Faculty of Exact Sciences, Tel Aviv University, Tel Aviv, Israel.

On behalf of the FCAL collaboration *

September 2008

Abstract

The linear collider community has set a goal to achieve a relative precision of 10^{-4} on the luminosity measurement at the ILC. This may be accomplished by constructing a finely granulated calorimeter, which will measure Bhabha scattering at small angles. In order to achieve the design goal, the geometrical parameters of the calorimeter are redefined. This is performed in a generalized manner, so as to facilitate future modifications, the need for which is foreseen, due to expected changes in the detector concept.

*List of members can be found at: http://www-zeuthen.desy.de/ILC/fcal/

1 Introduction

The focus of this study is the luminosity calorimeter (LumiCal) of the International Linear Collider (ILC). The requirement for LumiCal is to enable a measurement of the integrated luminosity with a relative precision of about 10^{-4} [1]. Bhabha scattering is used as the gauge process for the luminosity measurement. This is motivated by the fact that the cross-section of Bhabha scattering is large and dominated by electromagnetic processes, and thus can be calculated with very high precision [2, 3, 4, 5, 6].

The performance of LumiCal may be evaluated using several parameters; the precision with which luminosity is measured, the energy resolution, the ability to separate multiple showers, viability of the electronics readout, and finally, the integration of LumiCal into the detector. In the following, each of these criteria will be discussed.

Presently, two detectors are considered for the ILC with the pull-and-push scheme. Within the next half a year, letters of intent are expected. The European high energy committee, which has been working on the fifth version of the so-called "Large Detector Concept" (LDC) [7], has recently joined forces with the Japanese and American communities to promote the International Large Detector (ILD) [8] concept.

In the current ILD layout, LumiCal is placed 2.27 m from the interaction point (IP). LumiCal is a tungsten-silicon sandwich calorimeter. The inner radius of LumiCal is 80 mm, and its outer radius is 190 mm, resulting in a polar angular coverage of 35 to 84 mrad. The longitudinal part of the detector consists of layers, each composed of 3.5 mm of tungsten, which is equivalent to 1 radiation length (defined below) thickness. Behind each tungsten layer there is a 0.6 mm ceramic support, a 0.3 mm silicon sensors plane, and a 0.1 mm gap for electronics. LumiCal is comprised of 30 longitudinal layers. The transverse plane is subdivided in the radial and azimuthal directions. The number of radial divisions is 64, and the number of azimuthal divisions is 48. Figure 1 presents the segmentation scheme of a LumiCal sensor plane.

In the following study, it will be shown that for the present detector concept, the parameters listed above fulfill the requirement of best performance of LumiCal. Finally, the influence of making changes to the different parameters on the calorimeter performance will be summarized. This is necessary in order to facilitate setting an optimization procedure for future changes in the design of LumiCal.

2 Simulation Tools

The response of LumiCal to the passage of particles was simulated using MOKKA, version 06-05-p02 [9]. MOKKA is an application of a general purpose detector simulation package, GEANT4, of which version 9.0.p01 was used [10]. The MOKKA model chosen was LDC00_03Rp, where LumiCal is constructed by the LumiCalX super driver. The output of MOKKA is given in the LCIO format, which may be processed by MARLIN,

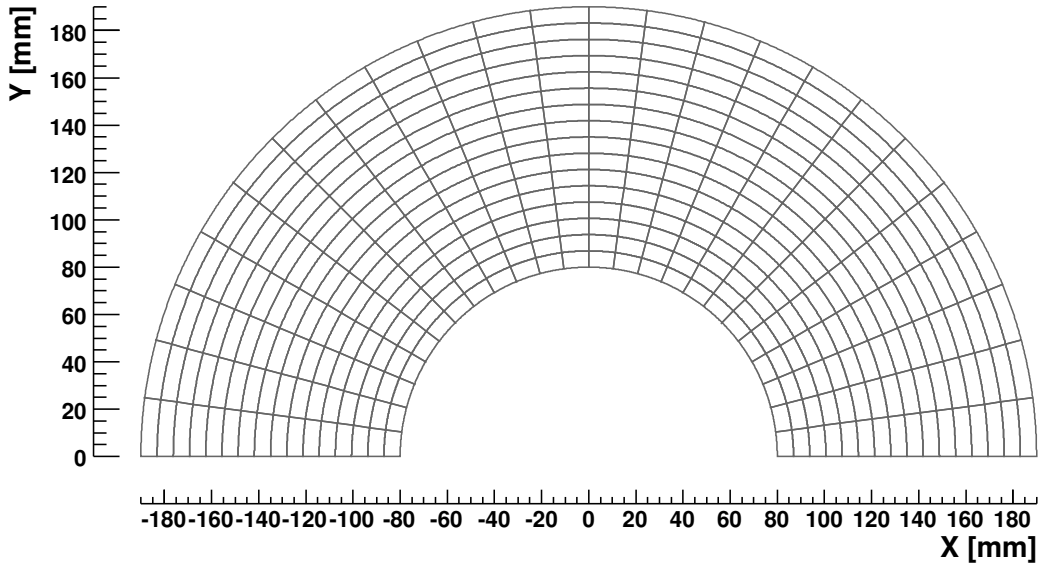

Figure 1: Half plane of LumiCal silicon sensors (every fourth radial segment is drawn).

a C++ software framework for the ILC software [11]. Version 00-09-08 of MARLIN was used.

3 Intrinsic Parameters

For small angles ($\leq 10^\circ$) Bhabha scattering is dominated by the t-channel exchange of a photon [12]. One can write the cross-section, σ_{B}, as

$$\frac{d\sigma_{\mathrm{B}}}{d\theta} = \frac{2\pi\alpha_{em}^2}{s}\frac{\sin\theta}{\sin^4(\theta/2)} \approx \frac{32\pi\alpha_{em}^2}{s}\frac{1}{\theta^3}\ , \tag{1}$$

where the scattering angle, θ, is the angle of the scattered lepton with respect to the beam, α_{em} is the fine structure constant, and s is the center-of-mass energy squared.

This means that the total Bhabha cross-section within the angular range $[\theta_{min}, \theta_{max}]$ is

$$\sigma_{\mathrm{B}} \sim \frac{1}{2}\left(\theta_{min}^{-2} - \theta_{max}^{-2}\right) \sim \frac{1}{2}\theta_{min}^{-2}, \tag{2}$$

where the θ_{max} dependence can be neglected. To measure the integrated luminosity, $\mathcal{L}$, one counts the number of Bhabha events, N_B, registered in LumiCal, using the respective integrated cross-section,

$$\mathcal{L} = \frac{N_B}{\sigma_B}. \tag{3}$$

3.1 Development of Electromagnetic Showers

When a high-energy electron or photon is incident on a thick absorber, it initiates an electromagnetic (EM) shower as pair production and bremsstrahlung generate more electrons and photons with lower energy. The characteristic amount of matter traversed for these related interactions is called the *radiation length*, X_0. It is both the mean distance over which a high-energy electron looses all but $1/e$ of its energy by bremsstrahlung, and $\frac{7}{9}$ of the mean free path for pair production by a high-energy photon [13]. The radiation length is also the appropriate scale length for describing high-energy electromagnetic showers. Electron energies eventually fall below the critical energy (defined below), and then dissipate their energy by ionization and excitation, rather than by the generation of more shower particles.

The transverse development of electromagnetic showers scales fairly accurately with the Molière radius, $R_{\mathcal{M}}$, given by [14]

$$R_{\mathcal{M}} = X_0 \frac{E_s}{E_c}\,, \tag{4}$$

where $E_s \approx 21$ MeV, and E_c is the *critical energy*, which is defined as the energy at which the ionization loss per radiation length is equal to the electron energy [15]. On average, only 10% of the energy of an EM shower lies outside a cylinder with radius $R_{\mathcal{M}}$ around the shower-center. Figure 2 shows the distribution of the distance around the shower-center, in which 90% of the integrated shower energy may be found, using 250 GeV electron showers. The distribution is centered around 14 mm.

3.2 Reconstruction of the Polar Angle

The polar angle is reconstructed by averaging over the individual cells hit in the detector, using the cell centers and a weight function, $\mathcal{W}_i$, such that

$$< \theta >= \frac{\sum_i \theta_i \cdot \mathcal{W}_i}{\sum_i \mathcal{W}_i}. \tag{5}$$

Weights are determined by the so-called logarithmic weighting [16], for which

$$\mathcal{W}_i = \max\{\ 0\ ,\ \mathcal{C} + \ln\frac{E_i}{E_{tot}}\}, \tag{6}$$

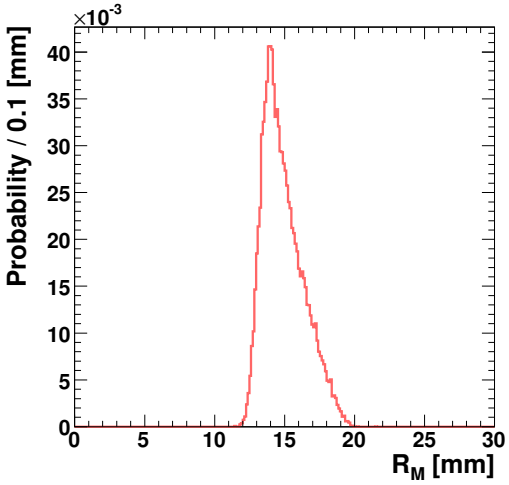

Figure 2: Distribution of $R_{\mathcal{M}}$, the distance around the global-shower center, in which 90% of the integrated shower energy may be found.

where E_i is the individual cell energy, E_{tot} is the total energy in all cells, and $\mathcal{C}$ is a constant. In this way, an effective cutoff is introduced on individual hits, and only cells which contain a high percentage of the event energy contribute to the reconstruction. This cut, which depends on the size of the different cells, and on the total absorbed energy, is determined by $\mathcal{C}$.

The polar resolution, σ_θ, and the polar bias, $\Delta\theta$, are, respectively, the root-mean-square and the most probable value of the distribution of the difference between the reconstructed and the generated polar angles. The existence of $\Delta\theta$ is due to the non-linear transformation between the global coordinate system of the detector, and the coordinate system of LumiCal, in which the shower position is reconstructed. There is an optimal value for $\mathcal{C}$, for which σ_θ is minimal. This is shown in Fig. 3a using 250 GeV electron showers. The corresponding values of $\Delta\theta$ are presented in Fig. 3b. Accordingly, the polar resolution and bias of LumiCal are $\sigma_\theta = (2.18 \pm 0.01) \cdot 10^{-2}$ mrad and $\Delta\theta = (3.2 \pm 0.1) \cdot 10^{-3}$ mrad, respectively.

3.3 Energy Resolution

LumiCal is designed in such a way that incident high energy electrons and photons deposit practically all of their energy in the detector. Prevention of leakage through the edges of LumiCal is possible by defining fiducial cuts on the minimal and on the maximal reconstructed polar angles of the particle showering in LumiCal, θ_{min} and θ_{max}. Stable energy resolution is the hallmark of well-contained showers. The relative energy resolution, σ_E/E, is usually parametrized as

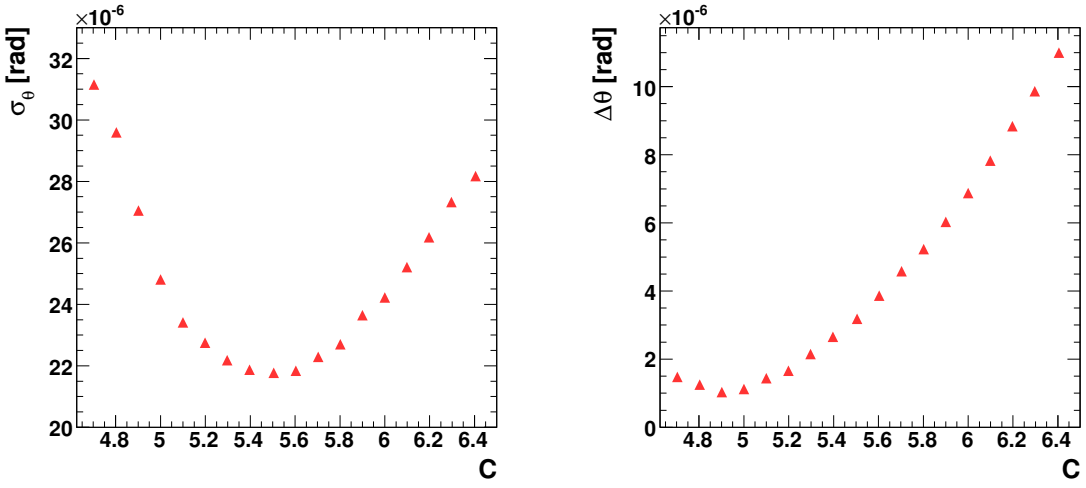

(a) (b)

Figure 3: The polar resolution, σ_θ, (a) and the polar bias, $\Delta\theta$, (b) as a function of the logarithmic weighing constant, $\mathcal{C}$, using 250 GeV electron showers.

$$\frac{\sigma_E}{E} = \frac{a_{res}}{\sqrt{E_{beam}\ (\mathrm{GeV})}}, \tag{7}$$

where E and σ_E are, respectively, the most probable value, and the root-mean-square of the signal distribution for a beam of electrons of energy E_{beam}. Very often the parameter a_{res} is quoted as resolution, a convention which will be followed here.

Figure 4a shows the energy resolution as a function of θ_{min} for 250 GeV electron showers. The maximal polar angle is kept constant. The best energy resolution is achieved for $\theta_{min} = 41$ mrad. A similar evaluation was done for a constant θ_{min} and a changing θ_{max}, resulting in an optimal cut at $\theta_{max} = 69$ mrad, as shown in Fig. 4b. The fiducial volume of LumiCal is thus defined to be within the polar angular range: $41 < \theta < 69$ mrad.

The dependence of the energy resolution on the energy of the electron which initiated the shower, E_{Gen}, is shown in Fig. 5. Only electron showers inside the fiducial volume of LumiCal are taken into account. The energy resolution is, therefore, $a_{res} = (20.66 \pm 0.01) \cdot 10^{-2}\ \sqrt{(\mathrm{GeV})}$.

3.4 Error on the Luminosity Measurement

The luminosity is measured with a statistical counting error,

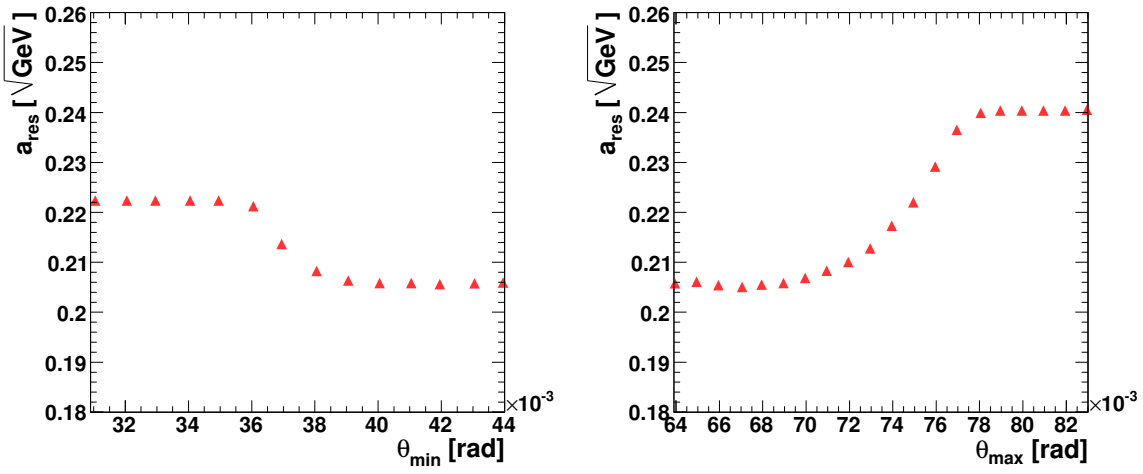

(a) (b)

Figure 4: The energy resolution, a_{res}, for 250 GeV electrons as a function of the minimal polar angle, θ_{min}, (a) and as a function of the maximal polar angle, θ_{max}, (b).

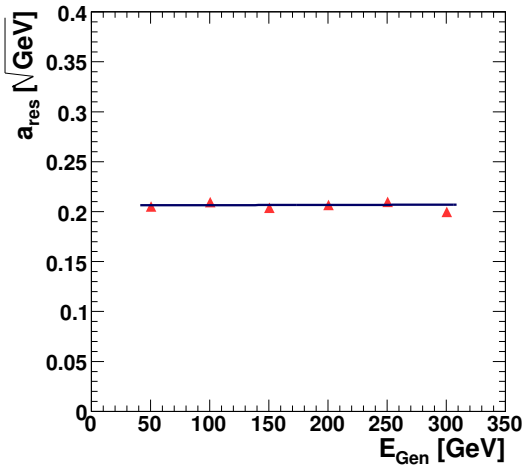

Figure 5: Dependence of the energy resolution, a_{res}, on the energy of the electron which initiated the shower, E_{Gen}.

$$\left(\frac{\Delta\mathcal{L}}{\mathcal{L}}\right)_{stat} = \frac{\Delta N_B}{N_B} = \frac{\sqrt{N_B}}{N_B} = \frac{1}{\sqrt{N_B}}\,, \tag{8}$$

and an additional error, which is proportional to the relative error on the Bhabha cross-section,

$$\left(\frac{\Delta\mathcal{L}}{\mathcal{L}}\right)_{rec} \approx 2\frac{\Delta\theta}{\theta_{min}}\,, \tag{9}$$

due to the reconstruction of the polar angle [17].

The analytic approximation of Eq. (9) has been shown to hold well in practice [18, 19]. Its implication is that $\Delta\theta$ and θ_{min} are the two most important parameters that affect the precision of the luminosity measurement. The steep fall of the Bhabha cross-section with the polar angle translates into significant differences in the counting rates of Bhabha events, for small changes in the angular acceptance range.

4 Geometrical Parameters of LumiCal

4.1 The Number of Radial Divisions

For different radial cell sizes one needs to re-optimize the logarithmic weighing constant, $\mathcal{C}$, of Eq. (6), as the distribution of deposited energy in a single cell changes for each case. The polar resolution and bias are plotted in Fig. 6 as a function of the angular cell size, ℓ_θ. In each case the appropriate optimal value of $\mathcal{C}$ was used. The respective values are presented in Table 1, along with the corresponding relative error in the luminosity measurement (Eq. (9)).

Both σ_θ and $\Delta\theta$ become smaller as the angular cell size decreases. The relative error in luminosity follows the same trend. This is due to the fact that the bounds on the fiducial volume do not strongly depend on the number of radial divisions. Consequently the minimal polar angle, θ_{min}, is the same (41 mrad) for all the entries of Table 1.

When the number of channels increases, problems, such as cross-talk between channels, power consumption issues and the need for cooling, arise. It is, therefore, advisable to keep the number of cells as low as possible. The chosen baseline number of 64 radial divisions is, therefore, a compromise between minimizing the relative luminosity error, and limiting the number of channels.

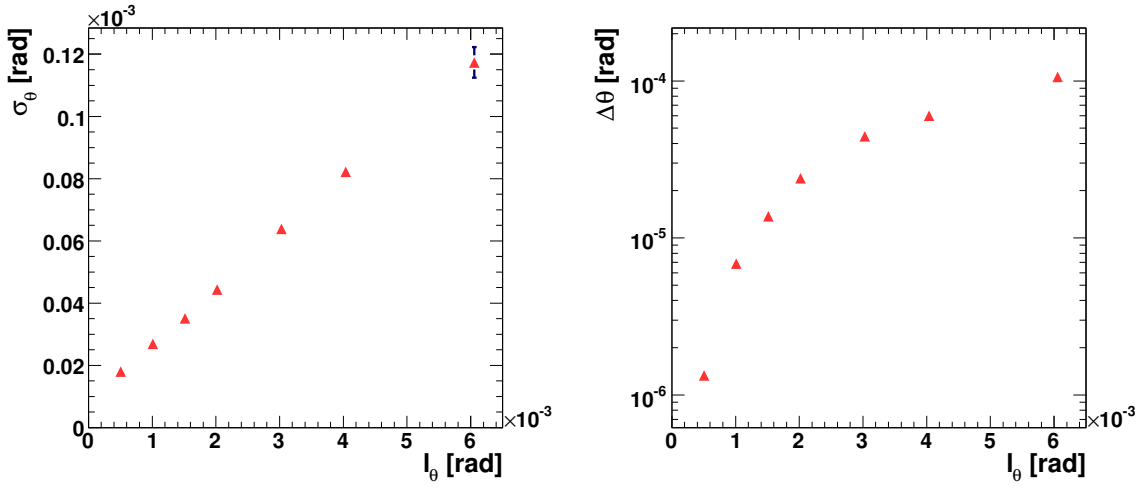

(a) (b)

Figure 6: The polar resolution, σ_θ, (a) and the polar bias, $\Delta\theta$, (b) for the appropriate optimal logarithmic weighing constants, as a function of the angular cell size, ℓ_θ. Electron showers of 250 GeV were used.

Δr	ℓ_θ [mrad]	σ_θ [mrad]	$\Delta\theta$ [mrad]	$\frac{2\Delta\theta}{\theta_{min}}$
96	0.5	$1.8 \cdot 10^{-2}$	$1.3 \cdot 10^{-3}$	$0.6 \cdot 10^{-4}$
64	0.8	$2.2 \cdot 10^{-2}$	$3.2 \cdot 10^{-3}$	$1.5 \cdot 10^{-4}$
48	1	$2.7 \cdot 10^{-2}$	$6.9 \cdot 10^{-3}$	$3.1 \cdot 10^{-4}$
32	1.5	$3.5 \cdot 10^{-2}$	$13.7 \cdot 10^{-3}$	$6.2 \cdot 10^{-4}$
24	2	$4.4 \cdot 10^{-2}$	$24 \cdot 10^{-3}$	$10.9 \cdot 10^{-4}$
16	2.5	$6.4 \cdot 10^{-2}$	$44.4 \cdot 10^{-3}$	$20.2 \cdot 10^{-4}$

Table 1: The polar resolution, σ_θ, and bias, $\Delta\theta$, for LumiCal with different numbers of radial divisions, Δr, corresponding to different angular cell sizes, ℓ_θ. The corresponding values of the relative error in the measurement of the luminosity are also shown.

4.2 The Number of Azimuthal Divisions

The number of azimuthal divisions does not affect the reconstruction of the polar angle. The energy resolution does not depend on the number of channels either, since energy contributions are integrated over all of the cells. In addition, the rounding errors, due to digitization of the signal, are small for the range of cell sizes which is being considered.

The importance of constraining the azimuthal cell size is in improving the resolving power of LumiCal, for distinguishing between multiple simultaneous showers. Strictly speaking, Born-level elastic Bhabha scattering never occurs. In practice, the process is always accompanied by the emission of electromagnetic radiation, $e^+e^- \to e^+e^-\gamma$. In a simplified picture, a Bhabha event may be depicted as occurring in three steps: emission of radiation from the initial particles, Bhabha scattering, and emission of radiation from the final particles. It should also be noted that the initial state radiation is mostly emitted in the direction of the beams and travels through the beampipe, thus remaining undetected[I].

The ability to distinguish between a final state radiative photon and its accompanying lepton is determined by the resolving capabilities of the detector, and is a function of the angular separation between the two particles. When the two can be separated, then the experimental measurement of the number of radiative photons can be compared with the theoretical prediction, and thus the theory can be partly tested.

A clustering algorithm has been developed in order to facilitate this goal [17, 20]. The conclusion was that there is a bound on the minimal azimuthal cell-length. This bound is defined in terms of $R_{\mathcal{M}}$, and so the respective number of azimuthal divisions depends on the distance of LumiCal from the IP. For the present distance of 2.27 m, 48 azimuthal divisions constitute the low bound.

4.3 The Structure of Layers

Each layer of LumiCal consists of 3.5 mm of tungsten, which is equivalent to one radiation length, X_0. A distribution of the energy deposited in a layer by 250 GeV electrons for a LumiCal of 90 layers is presented in Fig. 7a. Only 0.4% of the event energy is deposited beyond 30 layers. The distribution of the total event energy for 250 GeV electrons is plotted in Fig. 7b for a LumiCal with 90 layers and for a LumiCal with 30 layers. A small difference is apparent in the mean value of the distributions, but this bears no consequence, as the energy resolution is the same for both cases. It is, therefore, concluded that 30 layers (30 X_0) are sufficient for shower containment.

The Molière radius of LumiCal, $R_{\mathcal{M}}$, is plotted in Fig. 8a as a function of the gap between tungsten layers. Since a smaller $R_{\mathcal{M}}$ improves both the shower containment and the

[I] In the angular scattering range considered for the luminosity measurement, one can discard the effects of interference between the initial and final state radiation.

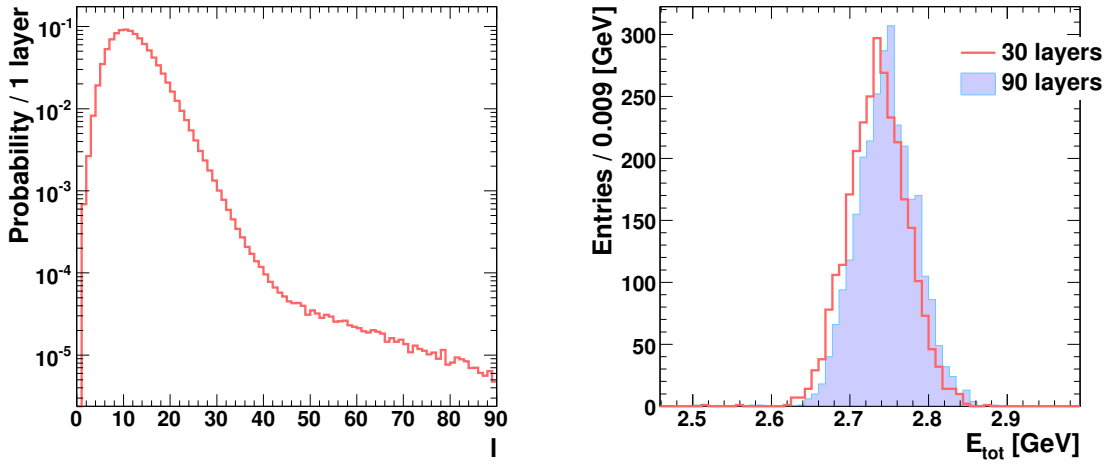

(a) (b)

Figure 7: (a) Normalized distribution of the energy deposited in LumiCal as a function of the layer number, ℓ, for a detector with 90 layers. (b) Comparison of the distribution of the total deposited energy, E_{tot}, for a 90 layer LumiCal with that of a 30 layer LumiCal, as denoted in the figure.

ability to separate multiple showers, the air gap should be made as small as possible. Figure 8b shows the dependence of the Molière radius on the tungsten thickness, d_{layer}. It is apparent that there is no significant change in $R_{\mathcal{M}}$ over the considered range.

Changing the thickness of tungsten layers increases the sampling rate. In order to ensure shower containment, the total number of layers must remain 30 X_0. Consequently, for smaller values of d_{layer}, more layers are needed, as shown in Table 2.

d_{layer} [mm]	2.0	2.5	3.0	3.5	4
N_{layer}	53	42	35	30	26

Table 2: The required number of LumiCal layers, N_{layer}, as a function of the thickness of each tungsten layer, d_{layer}.

Figure 9 shows the normalized distribution of the energy deposited per layer as a function of layer thicknesses, and the energy resolution, a_{res}, for each configuration. Figure 10 shows the corresponding polar resolution, σ_θ, and bias, $\Delta\theta$.

Due to the fact that more layers encompass the shower-peak area for smaller values of d_{layer}, the energy resolution is improved. The polar reconstruction and the Molière

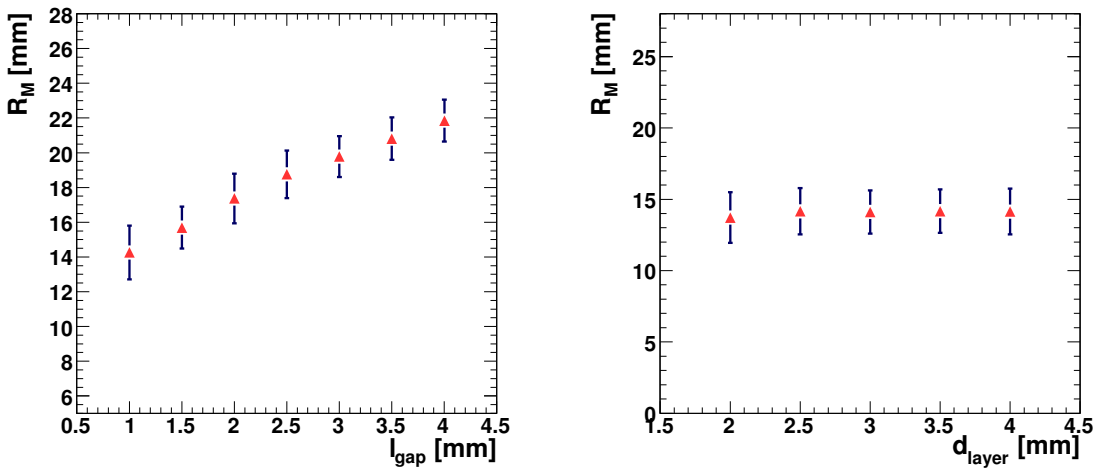

(a) (b)

Figure 8: The Molière radius of LumiCal, $R_{\mathcal{M}}$, as a function of the gap between tungsten layers, ℓ_{gap}, (a) and as a function of the thickness of each layer, d_{layer} (b).

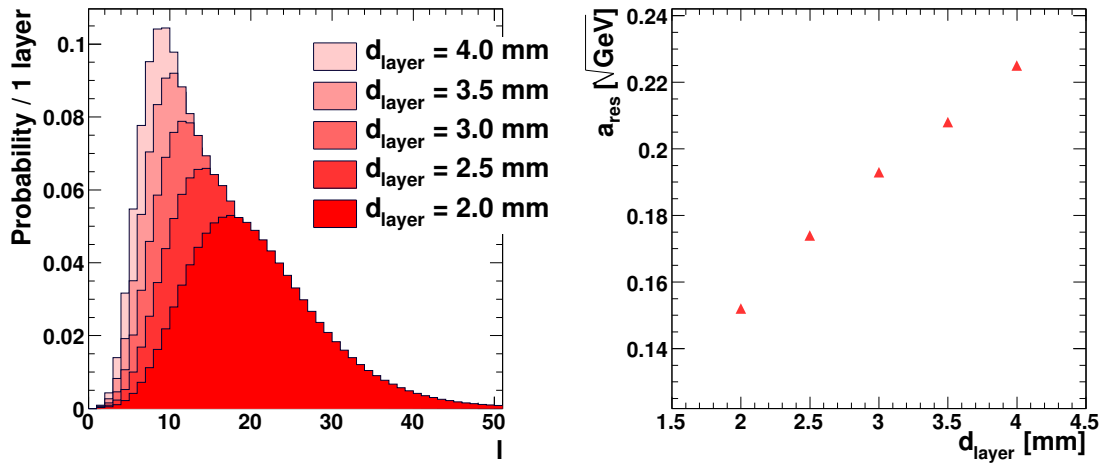

(a) (b)

Figure 9: (a) Normalized distribution of the deposited energy for 250 GeV electron showers as a function of the layer number, ℓ, for several layer thicknesses, d_{layer}, as denoted in the figure. (b) The energy resolution, a_{res}, as a function of the thickness of tungsten layers, d_{layer}, for electron showers of 250 GeV.

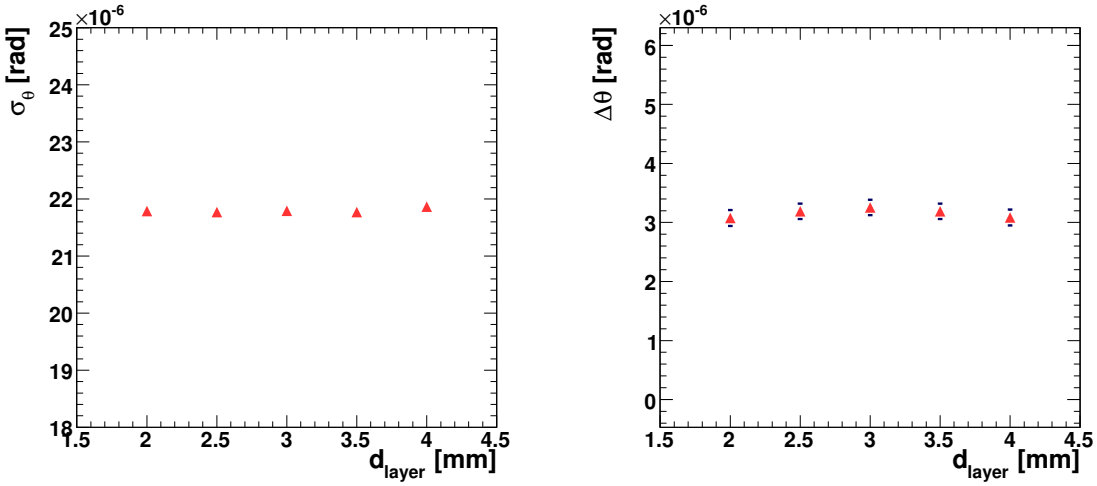

(a) (b)

Figure 10: The polar resolution, σ_θ, (a) and bias, $\Delta\theta$, (b) as a function of the thickness of a LumiCal layer, d_{layer}, using 250 GeV electron showers.

radius are not affected. The trade-off for choosing a given thickness of tungsten, is then between an improvement in a_{res} and the need to add more layers. Since increasing the number of layers also involves an increase in the cost of LumiCal, a clear lower bound on a_{res} needs to be defined, so as to justify the additional expense. Currently, $a_{res} \approx 0.21\ \sqrt{(\mathrm{GeV})}$ seems sufficient, and so $d_{layer} = 3.5$ mm was chosen.

4.4 Inner and Outer Radii

It is important to keep the total radial size of LumiCal, $\Delta R \equiv R_{max} - R_{min}$, large compared to the Molière radius, in order to ensure containment of showers, and to increase the capability of resolving multiple showers. For the choice of $\Delta R = 110$ mm ($\sim 8\ R_{\mathcal{M}}$), setting the values of the inner and outer radii, R_{min} and R_{max}, has several implications.

Since the Bhabha cross-section falls off quickly with the polar angle (see Eq. (1)), it is advantageous to set R_{min} as low as possible in order to increase the number of Bhabha events within the fiducial volume of LumiCal. Table 3 gives the integrated Bhabha cross-section, σ_{B}, in the fiducial volume defined by several choices of R_{min} and R_{max}, for a center-of-mass energy, $\sqrt{s} = 500$ GeV. The number of Bhabha events and the relative statistical error are calculated according to Eqs. (3) and (8), respectively. An integrated luminosity of 500 fb^{-1} was assumed. The relative error resulting from the polar reconstruction (Eq. (9)) is also shown in the table, where a polar bias, $\Delta\theta = 3.2 \cdot$

10^{-3} mrad (Table 1), and the appropriate minimal polar angles were used in each case.

$R_{min} \rightarrow R_{max}$ [mm]	θ_{min} [mrad]	θ_{max} [mrad]	σ_{B} [nb]	$\frac{\Delta N_B}{N_B}$	$\frac{2\Delta\theta}{\theta_{min}}$
$60 \rightarrow 170$	33	59	2.58	$2.8 \cdot 10^{-5}$	$1.9 \cdot 10^{-4}$
$70 \rightarrow 180$	37	64	1.98	$3.2 \cdot 10^{-5}$	$1.7 \cdot 10^{-4}$
$80 \rightarrow 190$	41	69	1.23	$4 \cdot 10^{-5}$	$1.5 \cdot 10^{-4}$
$90 \rightarrow 200$	50	74	0.86	$4.8 \cdot 10^{-5}$	$1.3 \cdot 10^{-4}$

Table 3: The fiducial volume bound by the minimal and maximal polar angles, θ_{min} and θ_{max}, for different inner and outer radii of LumiCal, R_{min} and R_{max}, and the integrated Bhabha cross-section, σ_{B}, for a center-of-mass energy, $\sqrt{s} = 500$ GeV. The two relative errors on the luminosity measurement, the statistical error and the one resulting from reconstruction of the polar angle, are also shown. The number of Bhabha events, N_B, is computed for an integrated luminosity of 500 fb^{-1}, and the polar bias used is $\Delta\theta = 3.2 \cdot 10^{-3}$ mrad.

As expected from Eq. (1), the number of Bhabha events increases for low values of R_{min}, thus decreasing the statistical error. As the polar bias depends on the angular cell size, which was kept constant, and not on the radii, the error resulting from the polar reconstruction decreases slightly for higher values of θ_{min}. Both effects contribute to the overall uncertainty in the luminosity measurement.

It should be noted here that in practice the counting rates of Bhabha events will be lower than presented in Table 3. This is due to the fact that the efficiency for counting Bhabha events is not 100% due to selection cuts [19]. This in itself does not add to the luminosity error, as long as the efficiency is known to high precision, but it does increase the statistical error[II].

The contribution of the error due to the polar bias also needs further consideration. In practice it will be possible to determine the polar bias using a test beam, and correct for this effect. The final error will then depend on how well one can correct for the bias, so that the values given in the table are an upper bound on the error.

At the ILC, the colliding electron and positron bunches disrupt one another [21]. Prior to the Bhabha scattering, the interacting particles are likely to have been deflected by the space charge of the opposite bunch, and their energies reduced due to the emission of beamstrahlung.

In the *detector integrated dipole* (DID) [22] field configuration, the magnetic field is

[II] For instance, for a pessimistic selection efficiency of roughly 50%, the error will increase by a factor of $\sqrt{2}$.

directed along the incoming beam lines with a kink at the transverse plane containing the IP. Conversely, the magnetic field may also be directed along outgoing beam lines with a kink at the IP plane, a configuration referred to as anti-DID. Figure 11 shows a projection of the energy of the beamstrahlung pairs on the face of LumiCal for the anti-DID and the DID magnetic field configurations of the accelerator, for the nominal accelerator operational parameters [23]. The two inner concentric black circles represent possible inner radii of 60 and 80 mm, while the outer circle is set at 190 mm. The beamstrahlung spectrum was generated using GUINEA-PIG [24].

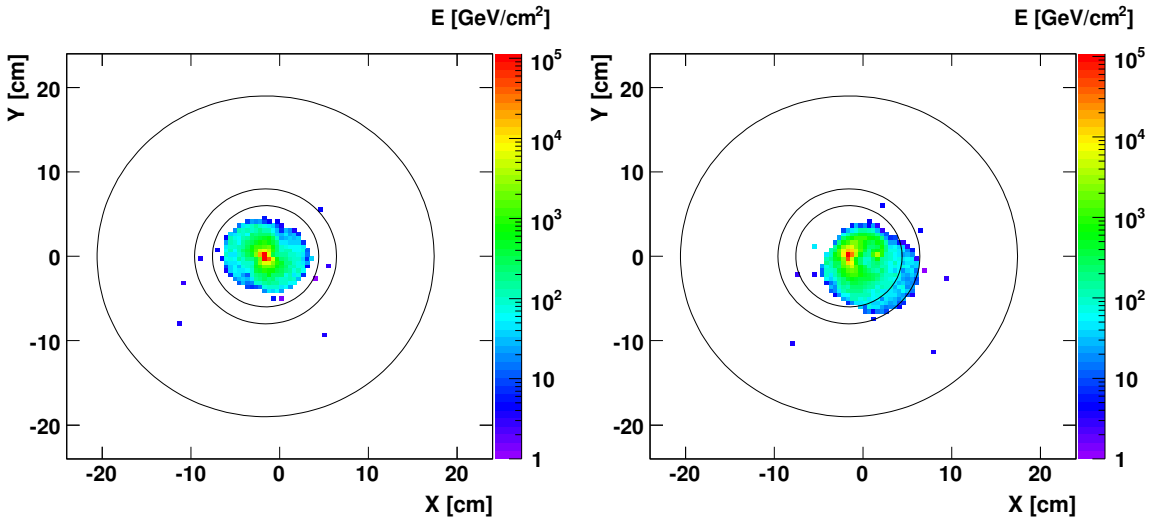

(a) (b)

Figure 11: Projection of beamstrahlung pair energies on the face of LumiCal for an anti-DID (a) and a DID (b) magnetic field setup, for the nominal accelerator operational parameters. The concentric circles represent possible inner LumiCal radii of 60 and 80 mm, and an outer radius of 190 mm.

For a DID field, the beamstrahlung pair distribution grazes LumiCal, while for the anti-DID case it does not, though the distribution comes close to the LumiCal inner edge. The effect of exposure to the extremely high energy dose will cause massive damage to the silicon sensors in a matter of months [25]. The anti-DID field is, thus, the better choice. The difference between the two distributions of Fig. 11 suggests that small fluctuations in the magnetic field from the nominal configuration will cause the pair distribution to become wider. It is, therefore, concluded that it would be preferable to add a safety margin to the minimal choice of the inner radius (60 mm).

It has also been shown [26] that for $R_{min} < 70$ mm there is a significant increase in the amount of backscattered particles from LumiCal to the inner detector (the TPC). This too constitutes a motivation for setting R_{min} at a higher value than 60 mm.

In conclusion, even given the realistic lower counting rate and no corrections of the polar bias, it is apparent that for the range of $R_{min} \rightarrow R_{max}$ given in Table 3, the relative error on the luminosity measurement is well within the design goal. Aiming to increase the available statistics as much as possible, while maintaining a safe distance from the beamstrahlung pairs, $R_{min} = 80$ mm was finally chosen.

5 Readout Scheme

For a given granularity of LumiCal, it is necessary to define the dynamical range of the electronics required to process the signal from the detector. Once the dynamical range is set, the digitization scheme depends on the ADC precision. The energy resolution depends on the digitization scheme.

A study was conducted, in which the response of LumiCal to the passage of minimum ionizing particles (MIP) and of 250 GeV electron showers was simulated [27]. These conditions represent the minimal and the maximal cases of energy deposition in LumiCal, respectively. The dynamical range of induced charge in a single LumiCal cell, C_{cell}, which was found, is $3.9 < C_{cell} < 6 \cdot 10^3$ fC. This result depends on the choice of cell size, as for larger LumiCal cells, the energy deposition in a single cell increases. The dependence of the signal on the size of LumiCal cells can be observed in Fig. 12a. The figure presents the distribution of collected charge per cell for 250 GeV electron showers for a LumiCal with 96 or 64 radial divisions, which correspond to angular cell sizes of 0.5 and 0.8 mrad, respectively. The distribution of the maximal charge collected in a single cell per shower for 250 GeV electrons is shown in Fig. 12b for the two radial division options.

The affect on the detector signal of digitizing the signal was also investigated in [27]. It was shown that a digitization constant larger than 8 bits is required in order to minimize the energy resolution, and that digitization of the signal does not produce energy bias.

6 Summary

In the following, the dependence of the various performance parameters on the geometry of LumiCal are summarized.

Energy resolution - The energy resolution depends on the containment of the EM shower, on the precision with which each cell is read out, and on the sampling rate of the shower.

- Containment of showers is achieved by keeping the total number of layers 30 X_0 thick, and imposing fiducial cuts on the polar angle of incident showers.

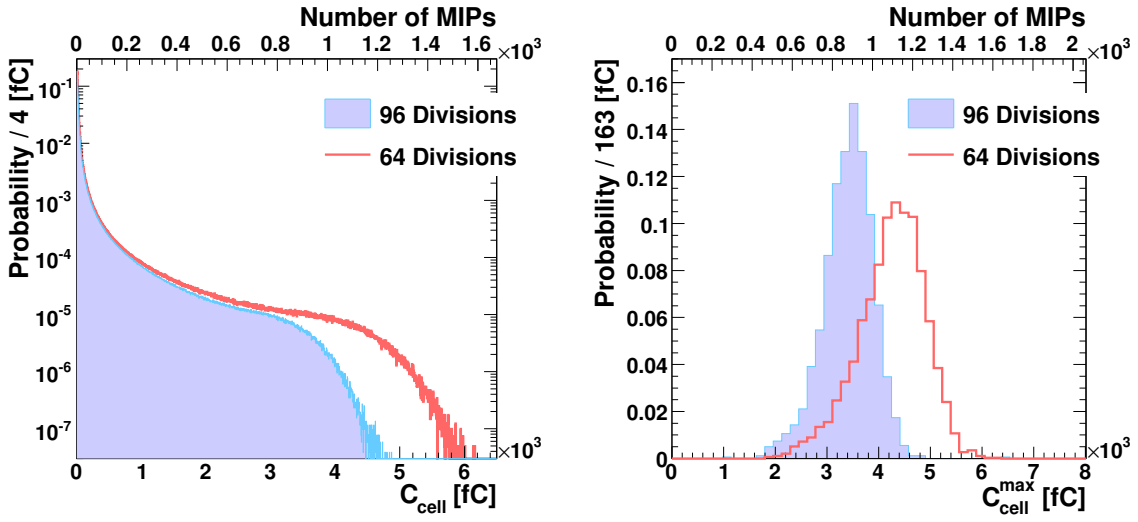

(a) (b)

Figure 12: (a) Normalized distribution of the charge deposited in a detector cell, C_{cell}, by 250 GeV electron showers for a LumiCal with 96 or 64 radial divisions, as denoted in the figure. (b) Normalized distribution of the maximal charge collected in a single cell per shower, C_{cell}^{max}, for 250 GeV electron showers for a LumiCal with 96 or 64 radial divisions, as denoted in the figure. In both figures a corresponding scale in units of MIPs is also shown.

- The accuracy of reading out cell energies is guarantied not to degrade the energy resolution, so long as a digitization scheme with high enough resolution is implemented. The restriction on the digitization constant depends on the size of the signal, which in turn depends on the size of LumiCal cells.

- The sampling rate of the shower is determined by the thickness of each tungsten layer. The best way to improve the energy resolution is to decrease the thickness of layers. One must increase the number of layers accordingly.

Molière radius - Keeping the Molière radius small improves both the shower containment, by relaxing the fiducial cuts, and the ability to resolve multiple showers. This may be done by decreasing the gap between tungsten layers to the minimal possible value. In general, the ability to separate multiple showers hinges upon the Molière radius being large in comparison to cell sizes, which puts low bounds on the number of radial and azimuthal divisions.

Inner and outer radii of LumiCal - The inner radius of LumiCal determines the minimal polar angle which is accessible by the calorimeter. Since the rate of Bhabha events falls off rapidly with the polar angle, it is preferable to decrease R_{min} as much as possible. The lower bound on R_{min} must be set such that the beamstrahlung pairs do not enter LumiCal, and the backscattering from LumiCal into the inner detector is acceptable. The outer radius of LumiCal is less important in terms of a gain in statistics, but the total radial size of LumiCal, $\Delta R = R_{max} - R_{min}$, must be kept large compared to the Molière radius.

Relative error on the luminosity measurement - Possible future changes in the position and size of LumiCal may affect its angular coverage and its angular cell size. This will influence the accuracy of the polar angle reconstruction, and accordingly the relative error on the luminosity measurement. The number of radial divisions must therefore be adjusted, so that the angular cell size remains ~ 1 mrad.

Dynamical range of the signal - Reducing the maximal signal of a single cell may be accomplished by increasing the number of cells. A low signal size brings about less rounding errors when digitizing the induced charge in a cell, and is also preferable from the readout electronics point of view. This change, however, carries the added complication of increasing the number of channels, which in turn hinders the readout, as discussed above.

Acknowledgments

This work is partly supported by the Commission of the European Communities under the 6th Framework Programme "Structuring the European Research Area", contract number RII3-026126, and by the Israeli Science Foundation.

References

[1] K. Mönig, "Physics Needs for the Forward Region." Talk given at the Zeuthen FCAL meeting, Aug. 2004.

[2] T. Becher and K. Melnikov, "Two-loop QED corrections to Bhabha scattering," *arXiv:0704.3582*.

[3] S. Actis, M. Czakon, J. Gluza, and T. Riemann, "Two-loop fermionic corrections to massive Bhabha scattering," *arXiv:0704.2400*.

[4] A. A. Penin, "Two-loop photonic corrections to massive Bhabha scattering," *Nucl. Phys. B, 734, 185 , arXiv:hep-ph/0508127*, 2006.

[5] M. Czakon, J. Gluza, and T. Riemann, "The planar four-point master integrals for massive two-loop Bhabha scattering," *Nucl. Phys. B, 751, 1 , rXiv:hep-ph/0604101*, 2006.

[6] S. Jadach, "Theoretical error of the luminosity cross section at LEP," *hep-ph/0306083*, 2003.

[7] "The Large Detector Concept." URL: http://www.ilcldc.org/.

[8] "The International Large Detector." URL: http://www.ilcild.org/.

[9] "MOKKA - a detailed GEANT4 detector simulation for the Future Linear Collider." URL: http://polywww.in2p3.fr/geant4/tesla/www/mokka/mokka.html.

[10] J. Allison *et al.*, "GEANT4 developments and applications," *IEEE Transactions on Nuclear Science, 53, No. 1, 270-278*, 2006.

[11] "MARLIN - a C++ software framework for ILC software." URL: http://ilcsoft.desy.de/portal/software_packages/marlin/index_eng.html.

[12] M. Caffo *et al.*, "Bhabha Scattering," *Z Physics at LEP1 , CERN Report 89-08, 1*, 1989. URL: http://documents.cern.ch/cgi-bin/setlink?base=cernrep&categ=Yellow_Report&id=89-08_v1.

[13] E. Segre, *Nuclei and Particles, New York, Benjamin, 65 ff*, 1964.

[14] W.-M. t. Yao, "Review of Particle Physics," *Journal of Physics G 33*, 2006. URL: http://pdg.lbl.gov.

[15] B. Rossi, *High Energy Particles, Prentice-Hall, Inc., Englewood Cliffs, NJ*, 1952.

[16] T. C. Awes *et al.*, "A simple method of shower localization and identification in laterally segmented calorimeters," *Nucl. Inst. Meth. A311, 130*, 1992.

[17] I. Sadeh, "Luminosity Measurement at the International Linear Collider." URL: http://alzt.tau.ac.il/~sadeh/mscThesis/iftachSadeh_mscThesis.pdf, 2008.

[18] R. Ingbir, "A Luminosity Detector for the International Linear Collider." URL: http://alzt.tau.ac.il/~ronen/, 2006.

[19] H. Abramowicz *et al.*, "A Luminosity Detector for the International Linear Collider," *LC-DET-2007-006*, 2007. URL: http://www-flc.desy.de/lcnotes/notes/LC-DET-2007-006.pdf.

[20] H. Abramowicz *et al.*, "A Clustering Algorithm for the Luminosity Calorimeter," *To be published as an LC-NOTE*. URL: http://alzt.tau.ac.il/~sadeh/.

[21] C. Rimbault *et al.*, "Impact of beam-beam effects on precision luminosity measurements at the ILC," *JINST 2 P09001*, 2007. URL: http://www.iop.org/EJ/abstract/1748-0221/2/09/P09001.

[22] A. Seryi and B. Parker, "Compensation of the effects of detector solenoid on the vertical beam orbit in NLC," *Phys.Rev.ST Accel.Beams 8, 041001*, 2005. URL: http://www-project.slac.stanford.edu/lc/ilc/TechNotes/LCCNotes/PDF/LCC-143.pdf.

[23] R. Heuer *et al.*, "Parameters for the Linear Collider." URL: http://www.fnal.gov/directorate/icfa/LC_parameters.pdf, 2003.

[24] D. Schulte, *TESLA-97-08*, 1996.

[25] I. Sadeh, "Calorimeters of the very forward region." Talk given at Joint ACFA Physics and Detector Workshop and GDE meeting on the International Linear Collider, URL: http://www.awa.tohoku.ac.jp/TILC08/, March 2008.

[26] C. Grah, "Pair background and the forward region," *Talk given at the October 2007 FCAL Collaboration Meeting, LAL-Orsay, France*. URL: http://events.lal.in2p3.fr/conferences/FCAL07/.

[27] H. Abramowicz *et al.*, "Revised Requirements on the Readout of the Luminosity Calorimeter," *EUDET-Memo-2008-08*, 2008. URL: http://www.eudet.org.